

Extending the Particle ESBGK Method to Diatomic Molecules including Quantized Vibrational Energies

M. Pfeiffer^{1, a)}

*Institute of Space Systems, University of Stuttgart, Pfaffenwaldring 29,
D-70569 Stuttgart, Germany*

(Dated: 5 September 2018)

The particle-based ellipsoidal statistical Bhatnagar-Gross-Krook (ESBGK) model is extended to diatomic molecules and compared with the Direct Simulation Monte Carlo (DSMC) method. For this an efficient method is developed that optionally allows the handling of quantized vibrational energies. The proposed method is verified with a gas in an adiabatic box relaxing from a non-equilibrium state to an equilibrium. It is shown that the analytical Landau-Teller expression as well as DSMC results agree very well with the new method. Furthermore, the method is compared with DSMC results and experimental measurements of a hypersonic flow around a 70° blunted cone. It is shown that the ellipsoidal statistical BGK compares very well with the DSMC results while saving up to a factor of ≈ 35.8 CPU time for this low Knudsen number case.

Keywords: DSMC, Ellipsoidal statistical BGK, BGK

^{a)}Electronic mail: mpfeiffer@irs.uni-stuttgart.de

I. INTRODUCTION

Simulations of non-equilibrium gas flows are still challenging especially if the simulation region includes dense and rarefied gas regions. The situation becomes even more complex for a molecular gas flow. In this case, non-equilibrium effects can also affect the inner energies of the molecules. CFD methods based on the Navier-Stokes equations cover a wide range of near equilibrium flows that are important for many practical applications. Nevertheless, the assumptions of the Navier-Stokes equations become invalid for rarefied non-equilibrium flows. Another approach of flow field simulation is the Direct Simulation Monte Carlo (DSMC) method. In this method, discrete particle collisions are used to mimic the convective and collision molecular process¹. Therefore, DSMC is able to handle non-equilibrium effects but becomes very expensive for small Knudsen number flows due to the fact that molecular events must be resolved in space and time within the mean free path and collision frequency, respectively.

The gap between the applicable flow regimes of both methods can be closed with different approaches. A short overview of these methods including advantages and disadvantages of these methods is given in Mirza et al.². The main focus in this paper is on the particle-based statistical Bhatnagar-Gross-Krook (BGK) method. This method is already used and coupled to DSMC in different applications like nozzle flow expansion³, micro channel flows⁴ or hypersonic shocks^{5,6}. Recently, an efficient method to handle arbitrary target distribution functions in the BGK context was presented⁶. However, it was shown that the energy conservation scheme becomes very important to produce the correct heat flux vectors, especially for non-symmetric distribution functions, e.g. resulting from the Shakhov model⁷. It was additionally shown that the ellipsoidal statistical BGK (ESBGK) model⁸ is very robust and produces good results concerning heat flux and shock structures.

In this paper, a relaxation model of internal energies for the ESBGK method will be presented. This work is based on the works of several authors^{3,5,9} but will allow the handling of quantised vibrational energies as typically used in the DSMC context. Furthermore, the energy conservation scheme is adapted, so that the relaxation process can also occur if only one particle is involved as opposed to the method proposed in several publications^{3,5}. First, the theory of the ESBGK model as well as internal energies are shortly discussed. Then, the implementation is described and subsequently verified by means of simple reservoir

simulations, where it is also compared to the DSMC method. Finally, the method is validated with a hypersonic flow around a 70° blunted cone including a shock structure.

II. THEORY

The Boltzmann equation describes the behaviour of gas with the corresponding distribution function $f = f(\mathbf{x}, \mathbf{v}, t)$ at position \mathbf{x} and velocity \mathbf{v}

$$\frac{\partial f}{\partial t} + \mathbf{v} \frac{\partial f}{\partial \mathbf{x}} = \left. \frac{\delta f}{\delta t} \right|_{Coll}. \quad (1)$$

In this equation, external forces are neglected. Furthermore, $\delta f / \delta t|_{Coll}$ is the collision term, which can be described by the Boltzmann collision integral

$$\left. \frac{\partial f}{\partial t} \right|_{Coll} = \int_{\mathbb{R}^3} \int_{S^2} \mathcal{B} [f(\mathbf{v}') f(\mathbf{v}'_*) - f(\mathbf{v}) f(\mathbf{v}_*)] d\mathbf{n} d\mathbf{v}_*. \quad (2)$$

Here, $S^2 \subset \mathbb{R}^3$ is the unit sphere, \mathbf{n} is the unit vector of the scattered velocities, \mathcal{B} is the collision kernel and the superscript ' denotes the post collision velocities. The multiple integration of this collision term makes is difficult to compute.

A. ESBGK Model

The ESBGK model approximates the collision term to a simple relaxation form, where the distribution function relaxes towards a target distribution function f^{ES} with a certain relaxation frequency ν :

$$\left. \frac{\partial f}{\partial t} \right|_{Coll} = \nu (f^{ES} - f). \quad (3)$$

The target velocity distribution function f^{ES} is given by

$$f^{ES} = \frac{n}{\sqrt{\det \mathcal{A}}} \left(\frac{m}{2\pi k_B T} \right)^{3/2} \exp \left[-\frac{m \mathbf{c}^T \mathcal{A}^{-1} \mathbf{c}}{2k_B T} \right] \quad (4)$$

with the anisotropic matrix

$$\mathcal{A} = \mathcal{I} - \frac{1 - Pr}{Pr} \left(\frac{3\mathcal{P}}{\text{Tr}[\mathcal{P}]} - \mathcal{I} \right). \quad (5)$$

The anisotropic matrix \mathcal{A} consists of the identity matrix \mathcal{I} and the pressure tensor \mathcal{P} ,

$$\mathcal{P} = \int \mathbf{c} \mathbf{c}^T f d\mathbf{v}, \quad (6)$$

which are both symmetric. Additionally, n is the particle density, m the particle mass, T the temperature and $\mathbf{c} = \mathbf{v} - \mathbf{u}$ the thermal particle velocity determined from the particle velocity \mathbf{v} and the average flow velocity \mathbf{u} ¹⁰. The ESBGK model reproduces the Maxwellian distribution in the equilibrium state as well as the correct moments of the Boltzmann equation. Furthermore, Andries et al.^{11,12} have shown that it fulfills the H-theorem. In the ESBGK model, the viscosity and the thermal conductivity are defined as

$$\mu = \frac{nk_B T}{\nu} Pr \quad K = \frac{c_P n k_B T}{\nu} \quad (7)$$

with the specific heat constant $c_P = 5k_B/2m$. Due to the fact that the viscosity depends on the Prandtl number, it is possible to reproduce the viscosity and thermal conductivity at the same time. Thus, the introduction of the Prandtl number as an additional parameter resolves the Prandtl number problem of the standard BGK model. The Prandtl number of molecules depends on inner degrees of freedom:

$$Pr = \frac{2(5 + \xi_R + \xi_V)}{15 + 2(\xi_V + \xi_R)} \quad (8)$$

with the rotational and vibrational degrees of freedom ξ_R , ξ_V , respectively.

As proposed by Gallis and Torczynski⁹, a symmetric transformation matrix \mathcal{S} with $\mathcal{A} = \mathcal{S}\mathcal{S}$ can be defined. Furthermore, a normalized thermal velocity vector \mathbf{C} is defined as such that $\mathbf{c} = \mathcal{S}\mathbf{C}$. Using these definitions, the argument of the exponential function in Eq. (4) becomes

$$\mathbf{c}^T \mathcal{A}^{-1} \mathbf{c} = (\mathcal{S}\mathbf{C})^T \mathcal{S}^{-1} \mathcal{S}^{-1} \mathcal{S}\mathbf{C} = \mathbf{C}^T \mathbf{C} \quad (9)$$

using $(\mathcal{S}\mathbf{C})^T = \mathbf{C}^T \mathcal{S}^T = \mathbf{C}^T \mathcal{S}$ due to the fact that \mathcal{S} is symmetric. Consequently, \mathcal{S} can transform a vector \mathbf{C} sampled from a Maxwellian distribution to a vector \mathbf{c} sampled from Eq. (4).

To determine the correct relaxation frequency ν , the well known exponential ansatz of the viscosity μ

$$\mu = \mu_{ref} \left(\frac{T}{T_{ref}} \right)^{\omega_{VHS}} \quad (10)$$

is used. Here, T_{ref} is a reference temperature, μ_{ref} the reference dynamic viscosity at T_{ref} ³ and ω_{VHS} is a parameter of the used variable hard sphere model (VHS). For a VHS gas the reference dynamic viscosity can be calculated with the VHS reference diameter d_{ref} of the particles:

$$\mu_{ref} = \frac{30\sqrt{mk_B T_{ref}}}{\sqrt{\pi}4(5 - 2\omega_{VHS})(7 - 2\omega_{VHS})d_{ref}^2}. \quad (11)$$

B. Diatomic Molecules

Next to the translational energy also the relaxation of internal vibrational and rotational energies must be treated in flows including molecules. The relaxation of the rotational temperature T_R and the vibrational temperature T_V is typically described with the Landau-Teller equation^{13–15}

$$\frac{dT_i}{dt} = -\nu_i(T_i - T_{Eq,i}), \quad i = R, V, \quad (12)$$

with the corresponding relaxation frequency ν_i and the equilibrium temperature $T_{Eq,i}$ for the rotational and vibrational energy. The equilibrium temperature in the Landau-Teller equation is the instantaneous translational cell temperature $T_{Eq,i} = T_{tr}$, which is calculated by using the equation of the unbiased sample variance as described in Sun and Boyd¹⁶

$$T_{tr} = \frac{m}{3k_B} \frac{\sum_{i=1}^N \mathbf{c}_i^2}{N-1}. \quad (13)$$

Eq. (13) results in $\xi_{tr} = 3(N-1)/N$ effective translational degrees of freedom per particle according to the equipartition theorem.

The rotational temperature T_R of the molecules in a diatomic rigid rotator model can be calculated using

$$T_R = \frac{2}{\xi_R k_B} \frac{\sum_{i=1}^N E_{R,i}}{N} \quad (14)$$

with the rotational energy $E_{R,i}$ of particle i and the rotational degrees of freedom $\xi_R = 2$.

The vibrational energy is described by the harmonic oscillator model

$$E_V = (j + 0.5)k_B\theta_V, \quad (15)$$

with the vibrational quantum number j and the characteristic vibrational temperature θ_V .

The analytical solution of the vibrational temperature in this model is given by

$$T_V = \frac{\theta_V}{\ln [1 + 1/(\langle E_V \rangle / k_B \theta_V - 0.5)]}, \quad \langle E_V \rangle = \frac{\sum_{i=1}^N E_{V,i}}{N}. \quad (16)$$

The vibrational degrees of freedom are depending on the vibrational temperature and can be calculated with

$$\xi_V(T_V) = \frac{2 \langle E_V \rangle}{k_B T_V} \quad \text{or} \quad \xi_V(T_V) = \frac{2\theta_V/T_V}{e^{\theta_V/T_V} - 1}. \quad (17)$$

The relaxation frequency ν_i of the inner degrees of freedom depends on the collision frequency of the gas ν_{coll}

$$\nu_{coll} = 2d_{ref}^2 n \sqrt{\frac{4\pi k_B T_{ref}}{m}} \left(\frac{T_{ref}}{T} \right)^{\omega_{VHS}} \quad (18)$$

according to $\nu_i = \nu_{coll}/Z_i$ with the collision number Z_i . Different models exist for the vibrational and rotational collision numbers Z_i , which can be found in Gimelshein et al.^{14,17}. As a simplification, constant collision numbers are assumed here. However, these constant numbers can easily be replaced with more sophisticated models in the proposed method.

III. IMPLEMENTATION

The ESBGK particle method is implemented in the PIC-DSMC code PICLas¹⁸ as described in detail in Pfeiffer⁶.

The main concept of the particle ESBGK method especially the energy and momentum conservation, is based on the works of^{3,5,9,19}. Here, particles are moved in a simulation mesh, collide with boundaries and the microscopic particle properties are sampled to calculate macroscopic values in the same manner as in DSMC. But in contrast to the DSMC method, the collision step with binary collisions between the particles is not performed. Instead, each particle in a cell relaxes with the probability

$$P = 1 - \exp[-\nu\Delta t] \quad (19)$$

according to Eq. (3) towards the target distribution. The relaxation frequency ν is evaluated in each time step for each cell from the definition of the viscosity of each model. The relaxation frequency directly depends on the cell temperature T , which is calculated from the particle information.

If a particle is chosen to relax, the new particle velocity is sampled from the target distribution. The detailed description of the sampling process for different target distributions (e.g. ESBGK or SBGK) can be found in Pfeiffer⁶. Here, an approach is used with an approximation of the transformation matrix \mathcal{S} of eq. (9) as described in previous studies^{3,5,9}

$$\mathcal{S}_{ij} = \delta_{ij} - \frac{1 - Pr}{2Pr} \left[\frac{m}{k_B T} \frac{N}{N - 1} (\mathcal{P}_{ij} - \hat{c}_i \hat{c}_j) - \delta_{ij} \right] \quad (20)$$

with

$$\hat{\mathbf{c}} = \int \mathbf{c} f d\mathbf{v}. \quad (21)$$

A. Relaxation of Internal Energies

To incorporate the internal energies in the algorithm, the Landau-Teller equation (12) is used in the same manner as the BGK collision term of Eq. (3). This means that each molecule relaxes the internal degree of freedom i to the equilibrium temperature Eq. (13) with the probability

$$P_i = 1 - \exp[-\nu_i \Delta t], \quad i = R, V, \quad (22)$$

irrespective of whether the particle is already chosen to relax according to Eq. (19). Whether or not this procedure reproduces the temperature according to the Landau-Teller equation depends on the used energy conservation scheme as described in Burt and Boyd³ and Tumuklu et al.⁵. The energy conservation is done by involving all N particles in a cell instead of only the relaxing particles. This scheme has shown to be more accurate in the case of small particle numbers per cell in different test cases⁶. The conditions for fulfilling energy and momentum conservation assuming only one species with mass m are

$$m \sum_{i=1}^N \mathbf{v}_i^* = m \sum_{i=1}^N \mathbf{v}_i \quad (23)$$

$$\sum_{i=1}^N \frac{m}{2} (\mathbf{v}_i^*)^2 + \sum_{i=1}^{N_R} E_{R,i}^* + \sum_{i=1}^{N_V} E_{V,i}^* = \sum_{i=1}^N \frac{m}{2} \mathbf{v}_i^2 + \sum_{i=1}^{N_R} E_{R,i} + \sum_{i=1}^{N_V} E_{V,i}. \quad (24)$$

Here, the superscript $*$ denotes the values after the energy conservation process and N_R as well as N_V are the numbers of the rotational and vibrational relaxing molecules as the result of Eq. (22), respectively. Eq. (24) yields the following equilibrium temperature after the energy conservation process:

$$T_{Eq}^* = \frac{3(N-1)T_{tr} + 2N_R T_R + \xi_V(T_V)N_V T_V}{3(N-1) + 2N + \xi_V(T_{Eq}^*)N_V}. \quad (25)$$

Unfortunately, this equilibrium does not necessarily fulfill the required condition of the Landau-Teller relaxation in Eq. (12). To overcome this problem, the relaxation probability of the internal energies is corrected with a parameter β_i as suggested by Burt³:

$$P_i = 1 - \exp[-\beta_i \nu_i \Delta t], \quad i = R, V. \quad (26)$$

To fulfill the Landau-Teller relaxation form, β_i will be chosen to

$$\frac{dT_i}{dt} = -\nu_i(T_i - T_{tr}) = -\beta_i \nu_i(T_i - T_{Eq}^*) \quad \Rightarrow \quad \beta_i = \frac{T_i - T_{tr}}{T_i - T_{Eq}^*}. \quad (27)$$

The solution of this equation system is solved numerically, due to the fact that T_{Eq}^* directly depends on β_R and β_V . For this purpose, the following system is solved

$$T_{Eq}^{*,n+1} = \frac{3(N-1)T_{tr} + 2P_R(\beta_R^n)NT_R + \xi_V(T_V)P_V(\beta_V^n)NT_V}{3(N-1) + 2P_R(\beta_R^n)N + \xi_V(T_{Eq}^{*,n})P_V(\beta_V^n)N} \quad (28)$$

$$\beta_i^{n+1} = \frac{T_i - T_{tr}}{T_i - T_{Eq}^{*,n+1}} \quad (29)$$

until $T_{Eq}^{*,n+1} - T_{Eq}^{*,n} < \varepsilon$ with the iteration step n and an accuracy ε . However, this equation system can be solved with an arbitrary method.

The new rotational energy $E'_{R,i}$ of molecules that are chosen for a rotational relaxation according to the corrected probability in Eq. (26) is reassigned to a value from a Boltzmann distribution

$$E'_{R,i} = -k_B T_{Eq}^* \ln(R_i) \quad (30)$$

with the random number R_i . This energy must be scaled additionally to fulfill the energy conservation.

The same method is also used for the vibrational energy:

$$E'_{V,i} = -\frac{\xi_V(T_{Eq}^*)}{2} k_B T_{Eq}^* \ln(R_i). \quad (31)$$

If the vibrational energy should be described by discrete quantum numbers, an additional step is necessary in the energy conservation process of $E_{V,i}$.

B. Energy and Momentum Conservation

The energy conservation process is performed in different steps and illustrated in Fig. 1. First of all, the energy conservation of the vibrational energy is performed. This must be done, if the vibrational energy is described in a quantized way. In the case of continuous vibrational energy, this fixed order is not necessary. In the used scheme, only translation-vibration ($T-V$) and translation-rotation ($T-R$) relaxation processes are allowed directly. Therefore, the energy E_{T-V}

$$E_{T-V} = \sum_{i=1}^N \frac{m}{2} \mathbf{c}_i^2 + \sum_{i=1}^{N_V} (E_{V,i} - 0.5k_B\Theta_V) \quad (32)$$

should be equally distributed over the translational $3(N-1)$ and vibrational $\xi_V(T_{Eq}^*)N_V$ degrees of freedom to fulfill energy conservation as well as the assumptions of Eq. (28). For

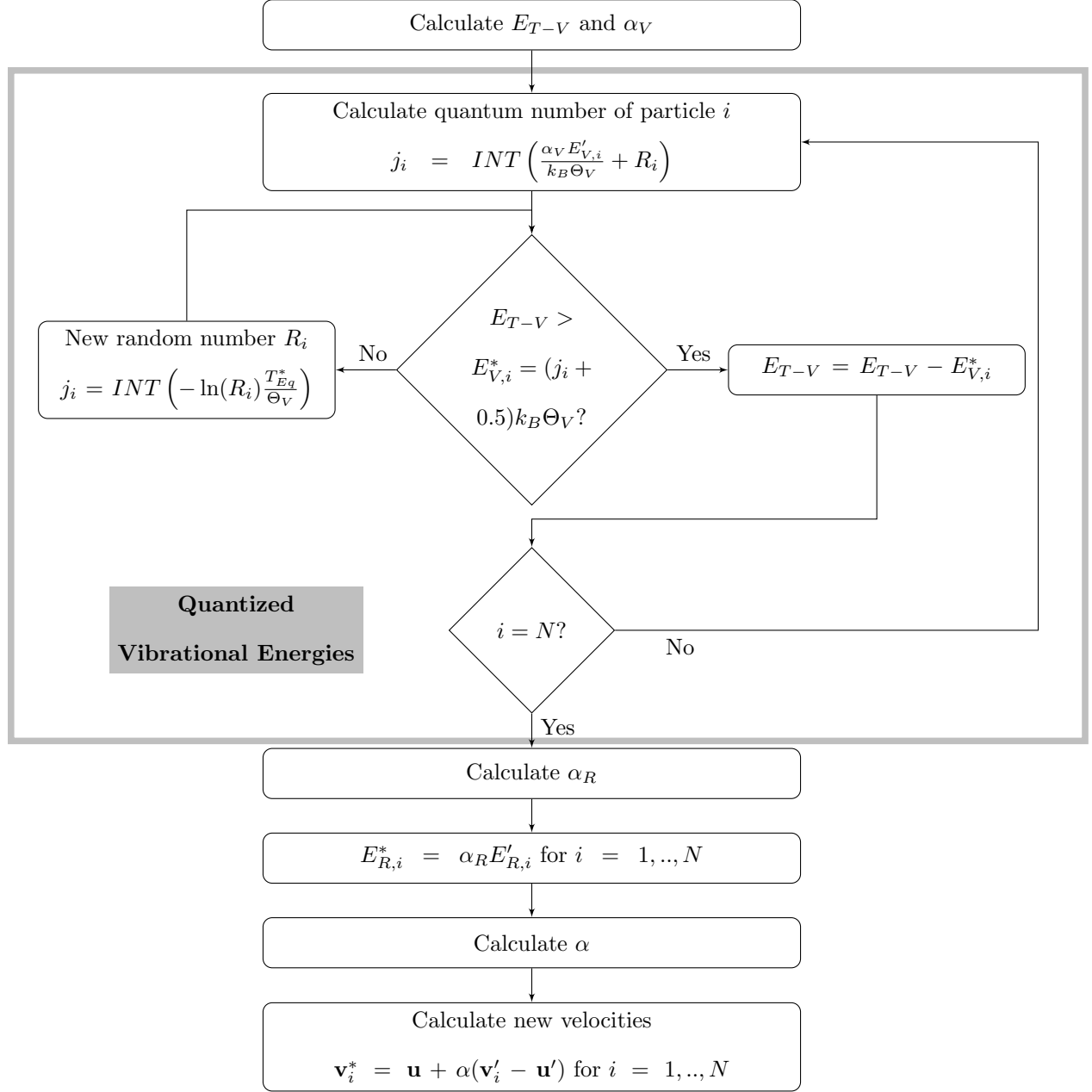


FIG. 1. Flow chart of energy conservation scheme.

this purpose, an α_V is defined with

$$E_{V,i}^* = \alpha_V E'_{V,i} + 0.5k_B \Theta_V. \quad (33)$$

The equal distribution over the DOFs is reached if

$$\alpha_V = \frac{E_{T-V}}{\sum_{i=1}^{N_V} E'_{V,i}} \left(\frac{\xi_V(T_{Eq}^*) N_V}{\xi_V(T_{Eq}^*) N_V + 3(N-1)} \right). \quad (34)$$

For continuous vibrational energies Eq. (34) is the final step, however, for quantized vibrational energies, further steps are necessary.

In the following, the quantized energy states for each particle are determined consecutively. The term $\alpha_V E'_{V,i}$ is reformulated to a quantum number using the random number R_i .

$$j_i = INT \left(\frac{\alpha_V E'_{V,i}}{k_B \Theta_V} + R_i \right). \quad (35)$$

With this quantum number it is checked whether the condition

$$E_{T-V} > E_{V,i}^* = (j_i + 0.5)k_B \Theta_V \quad (36)$$

is fulfilled. If this is the case, E_{T-V} is updated with $E_{T-V} = E_{T-V} - E_{V,i}^*$ and the next particle is processed. Otherwise, a new quantum number is calculated with the new random number R_i :

$$j_i = INT \left(-\ln(R_i) \frac{T_{Eq}^*}{\Theta_V} \right) \quad (37)$$

until the condition $E_{T-V} > E_{V,i}^*$ is fulfilled. Consequently, also the following particles in this algorithm can have a vibrational energy greater than zero. Note that for the following part of the energy conservation scheme, all $E_{V,i}^*$ must be subtracted from E_{T-V} also in the continuous vibrational energy case.

The energy conservation of the rotational and translational energies is achieved analogously to the vibrational energy. This means again that the energy E_{T-R}

$$E_{T-R} = E_{T-V} + \sum_{i=1}^{N_R} E_{R,i} \quad (38)$$

should be equally distributed over the translational and rotational degrees of freedom. Note that E_{T-V} includes the translational energy as well as the remaining vibrational energy in the quantized case. Therefore, the total system energy will be conserved with this scheme. The rotational energy is conserved using

$$E_{R,i}^* = \alpha_R E'_{R,i} \quad (39)$$

$$\alpha_R = \frac{E_{T-R}}{\sum_{i=1}^{N_R} E'_{R,i}} \left(\frac{2N_R}{2N_R + 3(N-1)} \right). \quad (40)$$

The momentum and energy conservation for the translational energy is done as described in the publications^{6,9} for the ESBGK model. Therefore, the final velocities of the particles are

$$\mathbf{v}_i^* = \mathbf{u} + \alpha(\mathbf{v}'_i - \mathbf{u}') \quad (41)$$

whether they relax or not. Here, $\mathbf{u} = \sum_{i=1}^N \mathbf{v}_i/N$ is the average flow velocity before the relaxation, \mathbf{v}'_i are the particle velocities after the relaxation but before the energy conservation process and $\mathbf{u}' = \sum_{i=1}^N \mathbf{v}'_i/N$. Note that, $\mathbf{v}'_i = \mathbf{v}_i$ if no relaxation occurs for particle i . Due to

$$\sum_{i=1}^N (\mathbf{v}'_i - \mathbf{u}') = 0, \quad (42)$$

eq. (41) ensures momentum conservation. Energy conservation is achieved by choosing α to

$$\alpha = \sqrt{\frac{E_{T-R}}{\sum_{i=1}^N \frac{m}{2} (\mathbf{v}'_i - \mathbf{u}')^2} \left(\frac{3(N-1)}{2N_R + 3(N-1)} \right)}. \quad (43)$$

IV. SIMULATION RESULTS

A. Reservoir simulations

The first verification case is a reservoir simulation in which particles are placed in an adiabatic box. Starting from a thermal non-equilibrium state at $t = 0$ s, a relaxation process is caused. After a certain amount of time, thermal equilibrium is reached as described by the Landau-Teller equation (12). If the translational-vibrational and translational-rotational relaxation is considered separately and an isothermal relaxation is assumed ($T_{Eq,i}(t) = T_{Eq,i}(t = \infty)$), it is possible to define an analytical solution of Eq. (12)^{13,20}:

$$\frac{E_i(\infty) - E_i(t)}{E_i(\infty) - E_i(0)} = e^{-t\nu_i}. \quad (44)$$

Here, the Landau-Teller equation is rewritten in the energy form. The verification simulation is done with N_2 . The particle density in the simulation is $n \approx 2 \cdot 10^{22} \text{ m}^{-3}$ (200 000 particles with a weighting factor $w = 10^7$ in a volume of $V = (4.6 \cdot 10^{-4})^3 \text{ m}^3$). Initial temperatures of the translational, rotational, and vibrational energies are $T_{\text{tr}} = 16000 \text{ K}$, $T_{\text{R}} = 8000 \text{ K}$, and $T_{\text{V}} = 8000 \text{ K}$, respectively. The characteristic vibrational temperature and species-specific constants for the variable hard sphere (VHS) model are summarized in Table I. The collision numbers are chosen to $Z_{\text{R}} = 5$ and $Z_{\text{V}} = 50$. For the comparison with the analytical solution, the translational temperature is fixed by reassigning the translational energy of the particles according to $T_{\text{tr}} = T_{Eq,i}(t = \infty) = 16000 \text{ K}$ after each time step. The rotational and vibrational relaxation is investigated separately by choosing $\nu_{\text{V}} = 0$ or $\nu_{\text{R}} = 0$, respectively. The results are shown in Fig. 2. The analytical solution and the results of the ESBGK

	Θ_V [K]	ω_{VHS}	T_{ref} [K]	d_{ref} [m]
N_2	3395	0.74	273	$4.17 \cdot 10^{-10}$

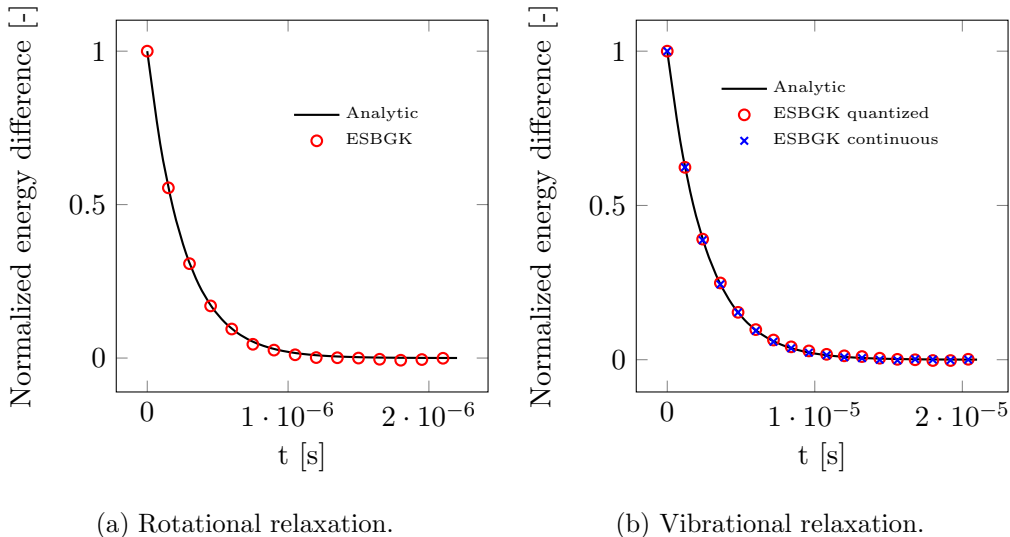
TABLE I. N_2 species constants.


FIG. 2. Comparison of BGK simulation results with analytical Landau-Teller solution.

method show a very good agreement for the rotational as well as vibrational relaxation. In the vibrational relaxation case, the quantized and the continuous model are used.

In the second test case, a simultaneous relaxation of the translational, rotational and vibrational temperature is investigated. For this, the reservoir simulation with the conditions described before is used again, only the initial temperatures are changed to $T_{tr} = 16000$ K, $T_R = 12000$ K, and $T_V = 8000$ K. The DSMC simulations are done using the prohibiting double relaxation method to reproduce the Landau-Teller equation as described in several works^{13,20}. The results of the DSMC and the ESBGK simulation using the quantized vibrational model is shown in Fig. 3. Excellent agreement is found between the DSMC and the BGK results.

B. 70° Blunted Cone

The 70° blunted cone described in Allègre et al.²¹ is chosen to validate the molecular ESBGK implementation, which was also used to validate the DSMC solver²². The geometry including the position of the thermocouples is shown in Fig 4. Due to the thermocouples, it

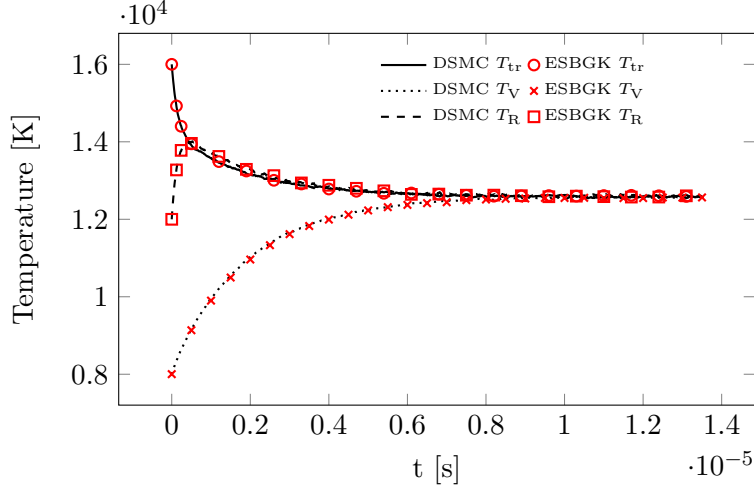


FIG. 3. Comparison of relaxation process of T_{tr} , T_R and T_V between DSMC and BGK.

is possible to compare simulation results with measured heat flux values on the surface.

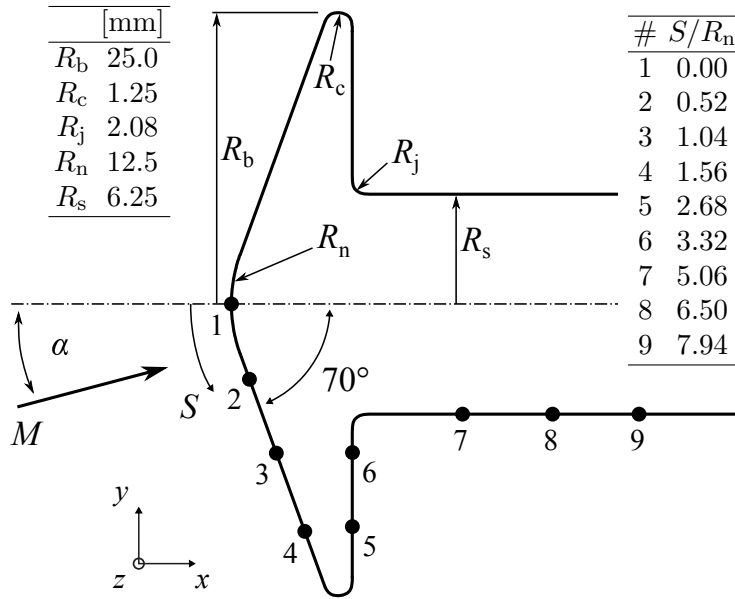
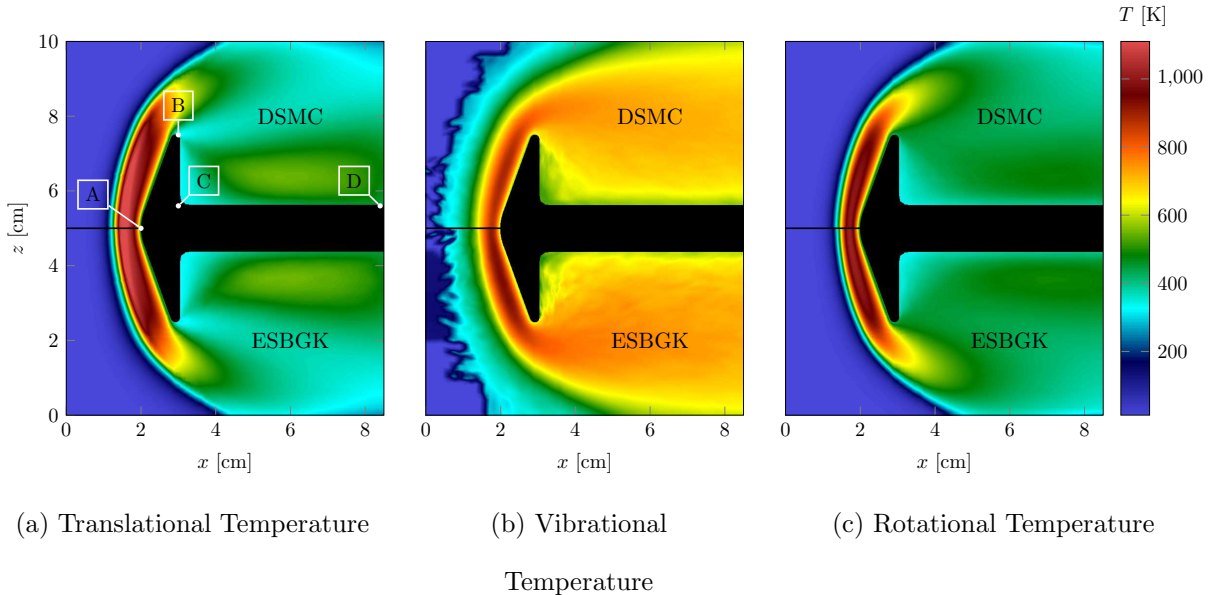


FIG. 4. 70° blunted cone geometry and positions of thermocouples.

The simulations were carried out for molecular nitrogen N_2 using the species constants of Table I with the inflow conditions of Table II. The two given inflow velocities are corresponding to angle of attacks of $\alpha = 0^\circ$ and $\alpha = 30^\circ$. Therefore, full 3D simulations are necessary. The Knudsen number of both cases is $Kn \approx 0.011$. The BGK method has similar requirements as the CFD method. To resolve the temperature and velocity gradients, a certain number of cells is required. Additionally, a certain number of particles per cell

	α [°]	\mathbf{v}_∞ [ms ⁻¹]	$T_{tr,V,R,\infty}$ [K]	n_∞ [m ⁻³]	Ma
Case 1	0	(1502.57, 0.0, 0.0) ^T	13.58	$1.115 \cdot 10^{21}$	20
Case 2	30	(1301.11, 0.0, 751.2) ^T	13.58	$1.115 \cdot 10^{21}$	20

TABLE II. Inflow conditions of 70° cone test case.

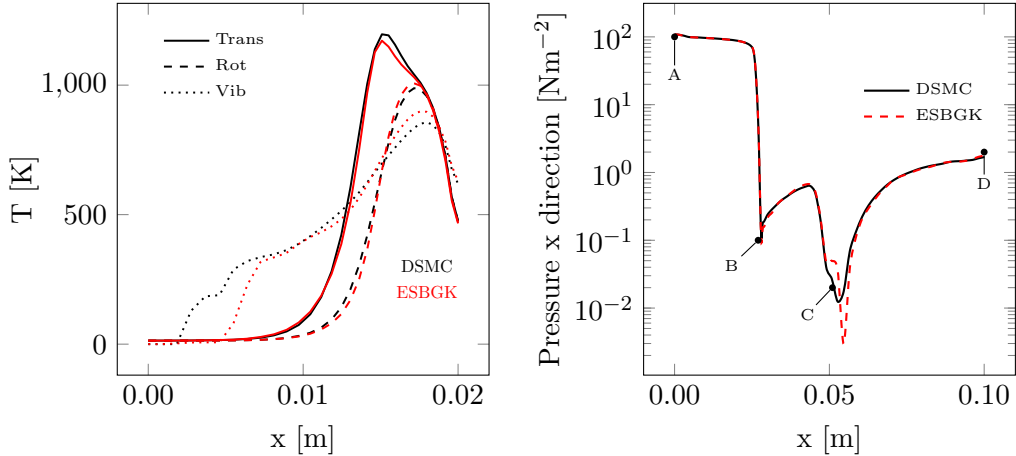

FIG. 5. Temperature plots of the flow field using DSMC and ESBGK for case 1 ($\alpha = 0^\circ$).

is required to represent the moments of the distribution function. Good results using the ESBGK model and the described energy conservation scheme are obtained with at least 7 to 10 particles per cell as described in Pfeiffer⁶. The time step can be found using a classic CFL condition with the stream velocity and the speed of sound^{2,23}.

Case 1 $\alpha = 0^\circ$

To resolve the mean free path and the collision frequency in the 3D DSMC simulation, a particle number of $N_{DSMC} = 4.5 \cdot 10^8$ and a time step of $\Delta t_{DSMC} = 5 \cdot 10^{-8}$ s are necessary. A comparison of the translational, rotational and vibrational temperatures in the flow field are shown in Fig. 5. The overall qualitative agreement is very good.

The temperature shock profile over the stagnation stream line is shown in detail in Fig. 6a. The overall agreement of the temperatures is very good. The biggest difference between the simulations is visible in the inflow area for the vibrational temperature. One reason for



(a) Temperature over stagnation stream line. (b) Pressure x direction on the surface.

FIG. 6. Simulation results of Case 1.

this difference is the statistical noise of the vibrational temperature in this region. The inflow is relatively cold, so that the quantized vibrational temperature is only slightly excited. Due to the fact that the ESBGK method needs much less particles ($N_{ESBGK} = N_{DSMC}/16$), the statistical noise is higher in the ESBGK method, which leads to the difference in the free stream inflow area.

The comparison of the heat flux and pressure in x-direction between DSMC and ESBGK are shown in Fig. 7 and 6b. Additionally, the positions and measurements of the thermocouples described in Fig. 4 are shown in Fig. 7. The points {A,B,C,D} in Fig. 6b correspond with the points depicted in Fig. 5a. The DSMC and ESBGK results show a very well agreement. Furthermore, the simulations match the measurements very well.

A comparison of the computational time is shown in Table III. The ESBGK method needs less particles ($N_{ESBGK} = N_{DSMC}/16$) and allows a larger time step $t_{ESBGK} = 2t_{DSMC}$. Therefore, the ESBGK model reduces the CPU time by a factor of ≈ 35.8 for this case compared with DSMC.

Case 2 $\alpha = 30^\circ$

The mean free path and the collision frequency in the 3D DSMC simulation of Case 2 $\alpha = 30^\circ$ are resolved using $N_{DSMC} = 4.2 \cdot 10^8$ and a time step of $\Delta t_{DSMC} = 5 \cdot 10^{-8}$ s. A

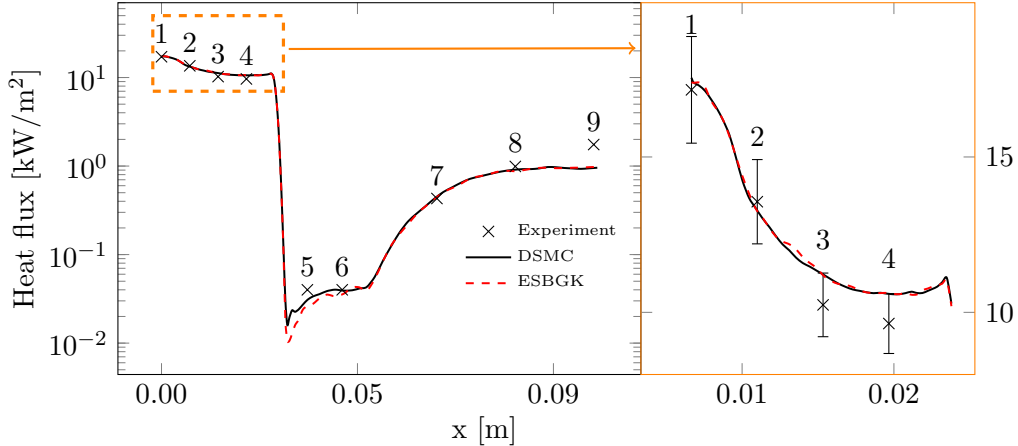


FIG. 7. Comparison of the heat flux on the surface for case 1.

	Particle Number N	Time step Δt [s]	CPU Time / 100 iterations [s]	CPU Time / $1 \cdot 10^{-5}$ s Simulation time [s]
DSMC	$4.5 \cdot 10^8$	$5 \cdot 10^{-8}$ s	1842	3684
ESBGK	$N_{DSMC}/16$	$2\Delta t_{DSMC}$	103	103

TABLE III. Comparison of CPU time between DSMC and ESBGK for Case 1. The CPU time is the time per node with 24 cores on a Intel Xeon CPU E5-2680 v3.

comparison of the translational, rotational and vibrational temperatures in the flow field is shown in Fig. 8. The overall agreement is again very good. The largest differences are visible in the wake region behind the shield. Furthermore, the vibrational temperature is slightly overestimated in the wake region. However, again much less particles are used in the ESBGK case, leading to greater statistical fluctuations and different results in the wake, especially for the quantized vibrational temperature.

The temperature shock profile over the black line depicted in Fig. 8a is shown in detail in Fig. 9a. The overall agreement of the temperatures is very good, whereby the largest difference is in the inflow area as previously discussed.

The comparison of the heat flux and pressure in x-direction between DSMC and ESBGK are shown in Fig. 10 and 9b. The DSMC and ESBGK results as well as the measurements show again a very well agreement.

A comparison of the computational time is shown in Table IV. The ESBGK method

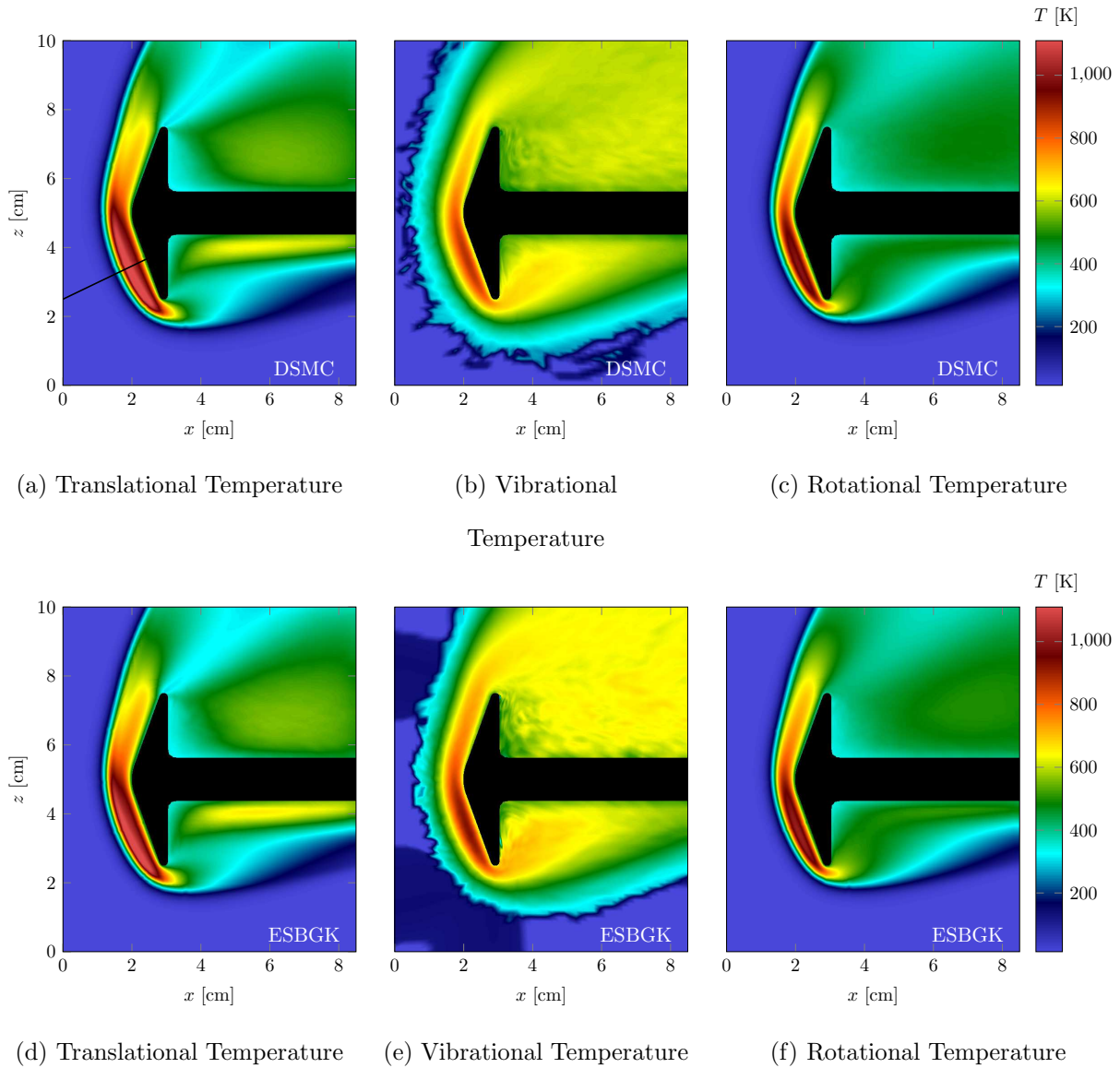


FIG. 8. Temperature plots of the flow field using DSMC and ESBGK for case 2 $\alpha = 30^\circ$.

needs less particles $N_{ESBGK} = N_{DSMC}/8$ and allows a larger time step $t_{ESBGK} = 2t_{DSMC}$. Therefore, the ESBGK model reduces the CPU time by a factor of ≈ 13.4 for case 2 compared with DSMC. In this case, more particles are needed compared to case 1 to correctly resolve the temperature gradients. Due to the angle of attack, a stronger bow shock forms in the front of the shield.

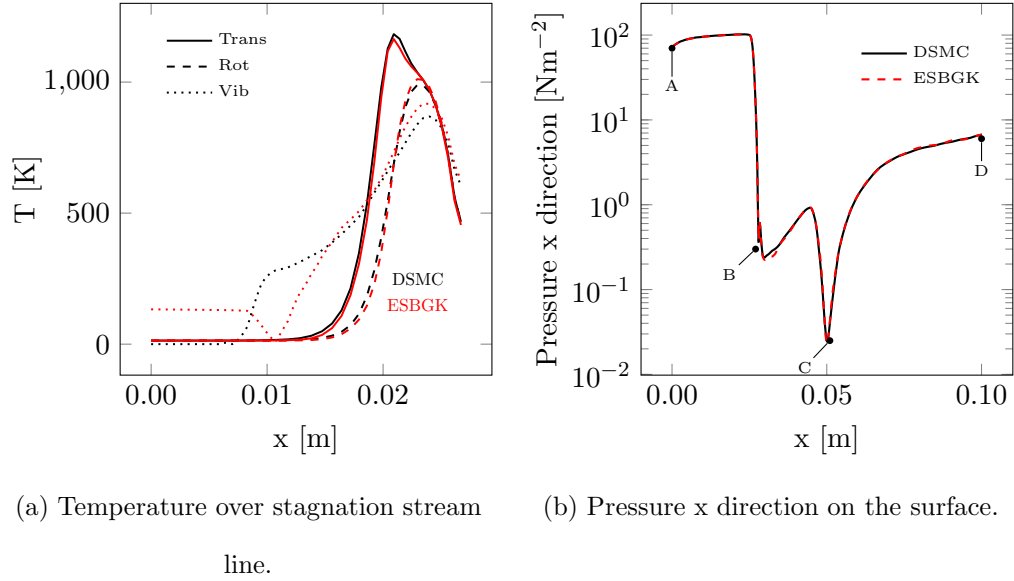


FIG. 9. Simulation results of Case 2.

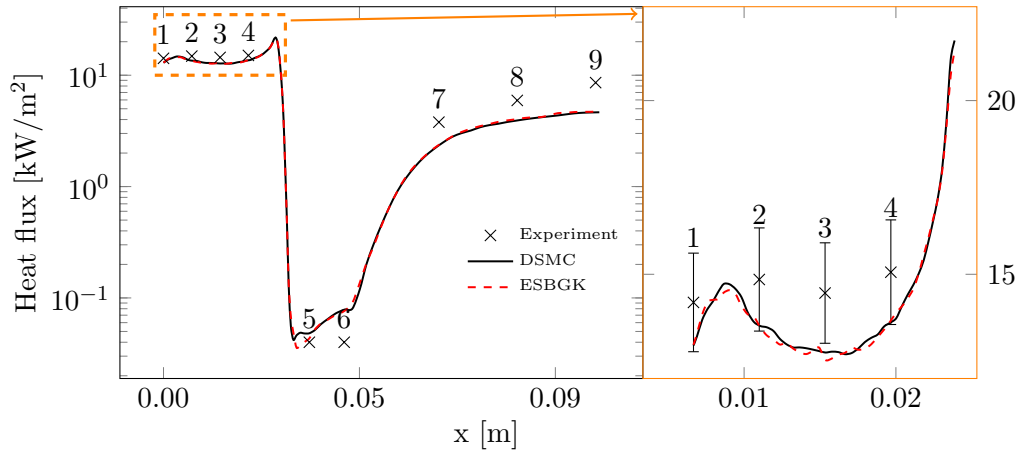


FIG. 10. Comparison of Heat flux on surface for Case 2.

	Particle Number N	Time step Δt [s]	CPU Time / 100 iterations [s]	CPU Time / $1 \cdot 10^{-5}$ s Simulation time [s]
DSMC	$4.2 \cdot 10^8$	$5 \cdot 10^{-8}$ s	1636	3272
ESBGK	$N_{DSMC}/8$	$2\Delta t_{DSMC}$	245	245

TABLE IV. Comparison of CPU time between DSMC and ESBGK for Case 2. The CPU time is the time per node with 24 cores on a Intel Xeon CPU E5-2680 v3.

V. CONCLUSION

A method is described that allows the efficient treatment of internal energies of diatomic molecules in the context of the particle-based ESBGK method. The shown method allows the handling of quantized as well as continuous vibrational energies. This allows the simulation of non-equilibrium low Knudsen number flows including diatomic molecules in a very efficient way compared with DSMC simulations.

The method was verified using an adiabatic box with a non-equilibrium initial condition. It was shown that the ESBGK method is able to match the analytical temporal behaviour described by the Landau-Teller equation as well as the DSMC results.

Further on, the ESBGK model was compared with DSMC simulations based on the hypersonic flow around a 70° blunted cone to evaluate the capabilities to capture the non-equilibrium effects in shock waves. It was shown that the heat flux values on the shield as well as the shock profiles fit the DSMC results very well. Furthermore it was shown that the ESBGK method can save up to a factor of ≈ 35.8 CPU time compared with DSMC for these problems.

This behavior is also very interesting for gas flows that cover a wide range of Knudsen numbers including continuum and rarefied gas regions as in nozzle expansion flows, where the coupling of the proposed ESBGK method with DSMC is beneficial in order to save computational time. The fact that DSMC and the investigated methods are both cell local Monte-Carlo based particle methods, makes a coupling very simple without the typical problems of hybrid CFD-DSMC methods.

A next step will be the extension of the proposed method to gas mixtures to allow the simulation of more complex flows.

ACKNOWLEDGMENTS

The author gratefully acknowledges the Deutsche Forschungsgemeinschaft (DFG) for funding this research within the project Partikelverfahren mit Strahlungslaser zur Simulation hochenthalper Nichtgleichgewichts-Plasmen (project number 93159129). The author also thanks the High Performance Computing Center Stuttgart (HLRS) for granting the computational time that has allowed the execution of the presented simulations.

REFERENCES

- ¹G. A. Bird, *Molecular Gas Dynamics and the Direct Simulation of Gas Flows*, 2nd ed. (Oxford University Press, New York, 1994).
- ²A. Mirza, P. Nizenkov, M. Pfeiffer, and S. Fasoulas, “Three-dimensional implementation of the Low Diffusion method for continuum flow simulations,” *Computer Physics Communications* **220**, 269 – 278 (2017).
- ³J. Burt and I. Boyd, “Evaluation of a particle method for the ellipsoidal statistical Bhatnagar-Gross-Krook equation,” in *44th AIAA Aerospace Sciences Meeting and Exhibit* (2006) p. 989.
- ⁴E. Titov, R. Kumar, D. Levin, N. Gimelshein, and S. Gimelshein, “Analysis of different approaches to modeling of nozzle flows in the near continuum regime,” in *AIP Conference Proceedings*, Vol. 1084 (AIP, 2008) pp. 978–984.
- ⁵O. Tumuklu, Z. Li, and D. A. Levin, “Particle ellipsoidal statistical Bhatnagar-Gross-Krook approach for simulation of hypersonic shocks,” *AIAA Journal* , 3701–3716 (2016).
- ⁶M. Pfeiffer, “Particle-based fluid dynamics: comparison of different bhatnagar-gross-krook models and the direct simulation monte carlo method for hypersonic flows,” Submitted.
- ⁷E. Shakhov, “Generalization of the Krook kinetic relaxation equation,” *Fluid Dynamics* **3**, 95–96 (1968).
- ⁸L. H. Holway Jr, “New statistical models for kinetic theory: methods of construction,” *The Physics of Fluids* **9**, 1658–1673 (1966).
- ⁹M. Gallis and J. Torczynski, “Investigation of the ellipsoidal-statistical Bhatnagar-Gross-Krook kinetic model applied to gas-phase transport of heat and tangential momentum between parallel walls,” *Physics of Fluids* **23**, 030601 (2011).
- ¹⁰P. L. Bhatnagar, E. P. Gross, and M. Krook, “A model for collision processes in gases. I. Small amplitude processes in charged and neutral one-component systems,” *Physical review* **94**, 511 (1954).
- ¹¹P. Andries, P. Le Tallec, J.-P. Perlat, and B. Perthame, “The Gaussian-BGK model of Boltzmann equation with small Prandtl number,” *European Journal of Mechanics-B/Fluids* **19**, 813–830 (2000).
- ¹²P. Andries and B. Perthame, “The ES-BGK model equation with correct Prandtl number,” in *AIP conference proceedings*, Vol. 585 (AIP, 2001) pp. 30–36.

- ¹³C. Zhang and T. E. Schwartzentruber, “Inelastic collision selection procedures for direct simulation monte carlo calculations of gas mixtures,” *Physics of Fluids (1994-present)* **25**, 106105 (2013).
- ¹⁴N. E. Gimelshein, S. F. Gimelshein, and D. A. Levin, “Vibrational relaxation rates in the direct simulation Monte Carlo method,” *Physics of Fluids* **14**, 4452 (2002).
- ¹⁵M. Pfeiffer, P. Nizenkov, A. Mirza, and S. Fasoulas, “Direct Simulation Monte Carlo modeling of relaxation processes in polyatomic gases,” *Physics of Fluids* **28**, 027103 (2016).
- ¹⁶Q. Sun and I. D. Boyd, “Evaluation of macroscopic properties in the direct simulation Monte Carlo method,” *Journal of Thermophysics and Heat Transfer* **19**, 329–335 (2005).
- ¹⁷B. L. Haas, D. B. Hash, G. A. Bird, F. E. Lumpkin, and H. A. Hassan, “Rates of thermal relaxation in direct simulation Monte Carlo methods,” *Physics of Fluids* **6**, 2191 (1994).
- ¹⁸C.-D. Munz, M. Auweter-Kurtz, S. Fasoulas, A. Mirza, P. Ortwein, M. Pfeiffer, and T. Stindl, “Coupled Particle-In-Cell and Direct Simulation Monte Carlo method for simulating reactive plasma flows,” *Comptes Rendus Mécanique* **342**, 662–670 (2014).
- ¹⁹M. Gallis and J. Torczynski, “The application of the BGK model in particle simulations,” in *34th Thermophysics Conference* (2000) p. 2360.
- ²⁰M. Pfeiffer, P. Nizenkov, A. Mirza, and S. Fasoulas, “Direct simulation Monte Carlo modeling of relaxation processes in polyatomic gases,” *Physics of Fluids* **28**, 027103 (2016).
- ²¹J. Allègre, D. Bisch, and J. C. Lengrand, “Experimental Rarefied Heat Transfer at Hypersonic Conditions over 70-Degree Blunted Cone,” *Journal of Spacecraft and Rockets* **34**, 724–728 (1997).
- ²²P. Nizenkov, P. Noeding, M. Konopka, and S. Fasoulas, “Verification and validation of a parallel 3d direct simulation monte carlo solver for atmospheric entry applications,” *CEAS Space Journal* **9**, 127–137 (2017).
- ²³M. Pfeiffer and M. Gorji, “Adaptive Particle-Cell algorithm for Fokker-Planck based rarefied gas flow simulations,” *Computer Physics Communications* **213**, 1 – 8 (2017).